Higgs branching ratio study for DBD detector benchmarking in ILD

Hiroaki Ono[1,*]

[1]*Nippon Dental University School of Life Dentistry at Niigata*

Precise measurement of Higgs boson branching ratios (BRs) is one of the key issues for the International Linear Collider (ILC) project to reveal a particles mass generation mechanism via Higgs and particles mass coupling relation. Even though the Higgs boson accurate measurement will be conducted at the center-of-mass (CM) energy of 250 GeV to adapt the 125 GeV of the mass of Higgs-like particle observed at the Large Hadron Collider (LHC) experiments [1, 2], ILC will also keep an extendability of CM energy up to 1 TeV to explore the new particles. In order to demonstrate the detector capability even at the 1 TeV, Higgs BRs measurement is also assigned as one of the detector benchmarking process for the Detailed Baseline Design (DBD) study. In this study, measurement accuracies of the product of the cross section and branching ratio into; two jet final state of $h \to b\bar{b}$, $c\bar{c}$, and gluons; four jet final state of $h \to WW^* \to 4j$, are evaluated with a full detector simulation adopting the International Large Detector (ILD) [3].

Keywords: ILC, Higgs boson, Branching ratio

I. INTRODUCTION

Higgs boson branching ratio measurement at the CM energy of 1 TeV in ILC project is one of the detector performance benchmarking processes listed in Detailed Baseline Design document (DBD) to demonstrate the detectors performance capability at higher energy.

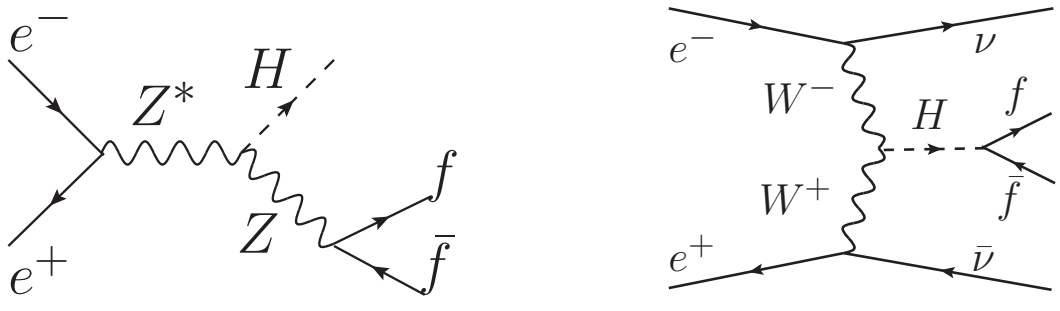

(a) (b)

FIG. 1: Higgs production process via (a) Higgs-strahlung ($e^+e^- \to Zh$) and (b) WW-fusion ($e^+e^- \to \nu_e\bar{\nu}_e h$)

*Electronic address: ono@ngt.ndu.ac.jp

At the CM energy below 500 GeV, Higgs boson mainly produced via Higgs-strahlung process: $e^+e^- \to Zh$ (Fig. 1 (a)) assuming a Higgs mass of 125 GeV and largest Higgs production cross section is obtained around the Zh production threshold of 250 GeV, as shown in Fig. 2. On the other hand, at the CM energy above 500 GeV, Higgs boson is mainly produced via WW-fusion process: $e^+e^- \to \nu_e\bar{\nu}_e h$ (Fig. 1 (b)) and much larger production cross section is obtained around the CM energy of 1 TeV than 250 GeV as shown in Fig. 2 (a) with assuming the $P(e^-,\ e^+) = P(-0.8,\ +0.2)$ left-handed beam polarization. Higgs production cross section assuming the right-handed beam polarization of $P(+0.8,\ -0.2)$ is also shown in Fig. 2 (b) and $\nu_e\bar{\nu}_e h$ production via WW-fusion process is suppressed at $\sqrt{s} = 1$ TeV.

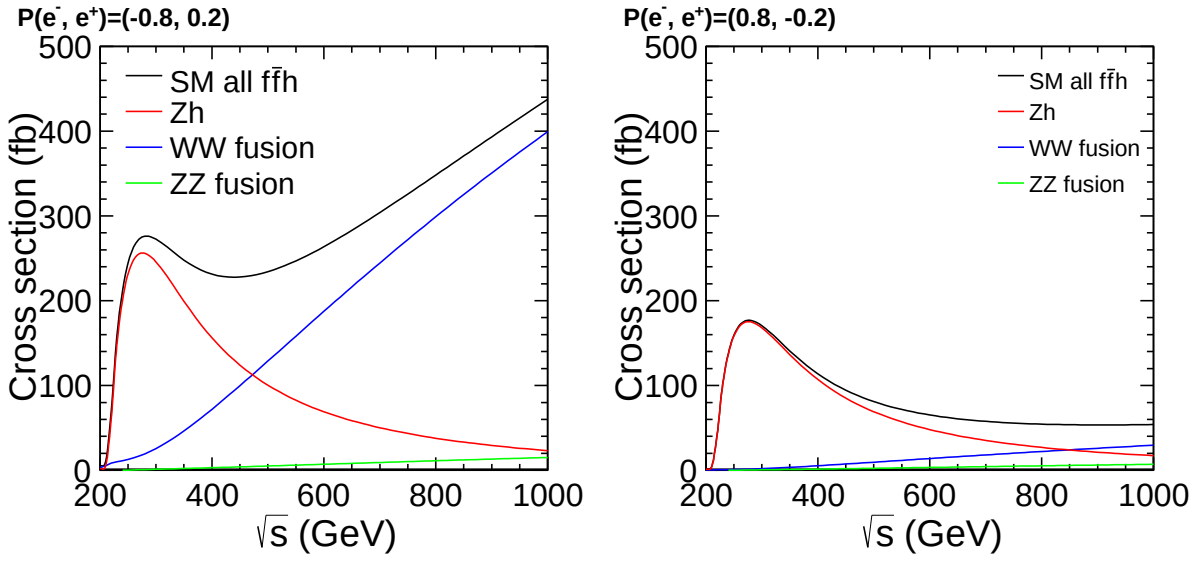

(a) (b)

FIG. 2: Higgs production cross sections as a function of CM energies at the Higgs mass of 125 GeV with (a) $P(e^-, e^+) = P(-0.8,\ +0.2)$ left-handed and (b) $P(+0.8,\ -0.2)$ right-handed beam polarizations.

In DBD benchmarking study, Standard Model (SM) Higgs BRs [4] are used to generate Higgs signal samples and Higgs BRs at different Higgs masses are shown in Fig. 3. Taking into account of the observation of Higgs-like particle in LHC experiments [1, 2], Higgs mass is selected as 125 GeV. From the Fig. 3, Higgs BRs measurement at the Higgs mass around 125 GeV is very suitable for accessing to the most of Higgs decay channels into both Fermions and Bosons. Higgs BRs at the Higgs mass of 125 GeV are summarized in Table I and Higgs mainly decays into $b\bar{b}$.

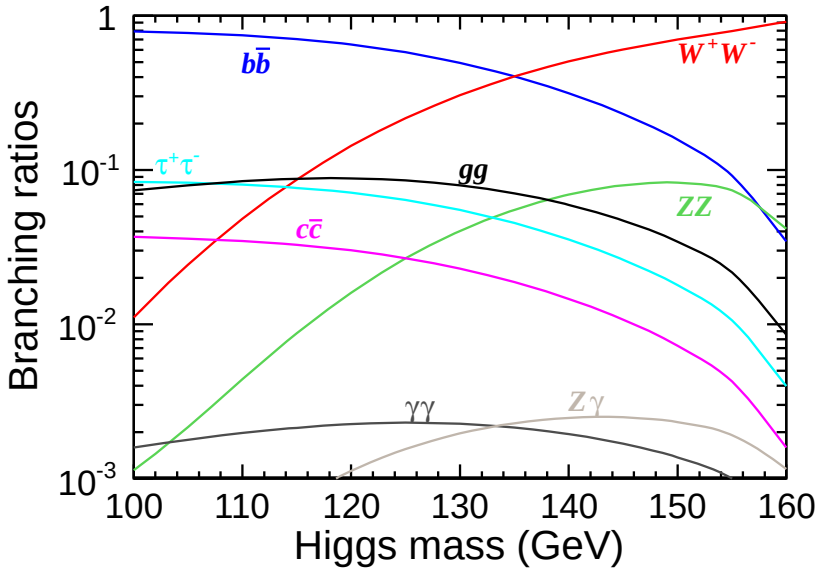

FIG. 3: SM Higgs BRs as a function of Higgs mass referred from [4].

TABLE I: Higgs BRs for each particle at the Higgs mass of 125 GeV.

Higgs decay channels	$b\bar{b}$	$c\bar{c}$	gg	WW*	$\mu^+\mu^-$	$\tau^+\tau^-$	ZZ*	$\gamma\gamma$	$Z\gamma$
Higgs BRs	57.8%	2.7%	8.6%	21.6%	0.02%	6.4%	2.7%	0.23%	0.16%

II. SIMULATION AND RECONSTRUCTION TOOLS

A. ILD standard samples for DBD

In the detector benchmarking study for ILD DBD, standard Higgs signals ($f\bar{f}h$) selecting its mass of 125 GeV and SM background samples were centrally generated employing `whizard 1.95` [5]. All the generated standard signal and background samples are summarized in Table II.

From the Table II, Higgs is mainly produced via WW-fusion process thus large missing energy and transverse momentum is in final state forming multi-jets. Taking into account of this final state, $e\nu W$ and $\nu\nu Z$, WW/ZZ final state from $e^+e^- \rightarrow$ 4f channels are supposed to be major background, which makes mass peak around Z and closed to the Higgs mass peak. $e\gamma \rightarrow \nu qq$ from $e\gamma \rightarrow$ 3f channel also considered as major background, since electrons or photons escapes to the beam pipe, invisible particles contribute as missing energy. Two photon backgrounds of $\gamma\gamma \rightarrow \nu\nu qq$ are also considered as similar final state of signal channel.

Simulation and reconstruction were performed employing latest `ilcsoft v01-16-p03` [6]. Gen-

TABLE II: Production cross sections and expected number of events of Higgs and supposed SM backgrounds in this study assuming the integrated luminosity of 500 fb^{-1} for each beam polarization $P(e^-, e^+) = P(\mp 0.8, \pm 0.2)$.

	Higgs signals ($M_h = 125$ GeV, $\sqrt{s} = 1$ TeV)			
Processes	$\sigma(-0.8, +0.2)$ (fb)	$\sigma(+0.8, -0.2)$ (fb)	N$(-0.8, +0.2)$	N$(+0.8, -0.2)$
$\nu\bar{\nu}$h	404	33	202,022	16,549
$q\bar{q}$h	18	12	8,885	6,058
$\ell\ell$h	25	16	12,501	8,089
$f\bar{f}$h	447	61	223,408	30,697

Processes	SM backgrounds ($\sqrt{s} = 1$ TeV)			
$e^+e^- \to 2f$	7,780	5,399	3.9×10^6	2.7×10^6
$e^+e^- \to 4f$	27,028	13,060	13.5×10^6	6.5×10^6
$e^+e^- \to 6f$	693	239	0.4×10^6	0.1×10^6
$e\gamma \to 3f$	460,783	398,016	230.4×10^6	199.0×10^6
$e\gamma \to 5f$	1,370	872	0.8×10^6	0.4×10^6
$\gamma\gamma \to 4f$	3,137	3,137	$1,6 \times 10^6$	1.6×10^6

erated signals were passed through the detector simulation in `Mokka` [7] employing the latest ILD detector model of `ILD_o1_v05`. Simulated hits were digitized and reconstructed in the `MarlinReco` [8].

III. SGV fast simulation

Due to the time limitation of the full detector simulation and reconstruction, several background samples are separately simulated using SGV fast simulator [9], which can reproduce the Mokka detector simulation well. Higgs signal and $e^+e^- \to 2f,\ 4f,\ 6f$ channels are fully simulated and reconstructed by full simulation but other $e\gamma \to 3f,\ 5f$, and $\gamma\gamma \to 4f$ are simulated with SGV fast simulator. In this study, ILD standard generated and reconstructed samples are used. At the analysis stage, each sample is scaled to be the integrated luminosity of 500 fb^{-1} or 1 ab^{-1} and generated 100% polarized samples are mixed with appropriate factors to obtain the expected $P(e^-,\ e^+) = P(\mp 0.8,\ \pm 0.2)$ polarized beam condition.

A. Beam related $\gamma\gamma \to$ hadron background

At the CM energy of 1 TeV, beam induced backgrounds are not negligible even in the lepton collider and 4.1 events of $\gamma\gamma \to$ hadron backgrounds are estimated per one bunch crossing. For each simulated sample, $\gamma\gamma \to$ hadron backgrounds are overlaid on the simulated hits. But note that current reconstructed samples using SGV are not overlaid $\gamma\gamma$ backgrounds, but same k_t algorithm is applied at the reconstruction stage. To treat these beam related backgrounds, k_t jet clustering algorithm implemented in `FastJet` [10] package is employed, which is commonly used for the hadron collider experiment to treat the beam related backgrounds.

In exclusive k_t jet algorithm, beam induced particles are combined as beam jet ($J_{\rm beam}$) and not used as clustered jets [11]. After applying the k_t jet clustering, beam related PFOs mainly

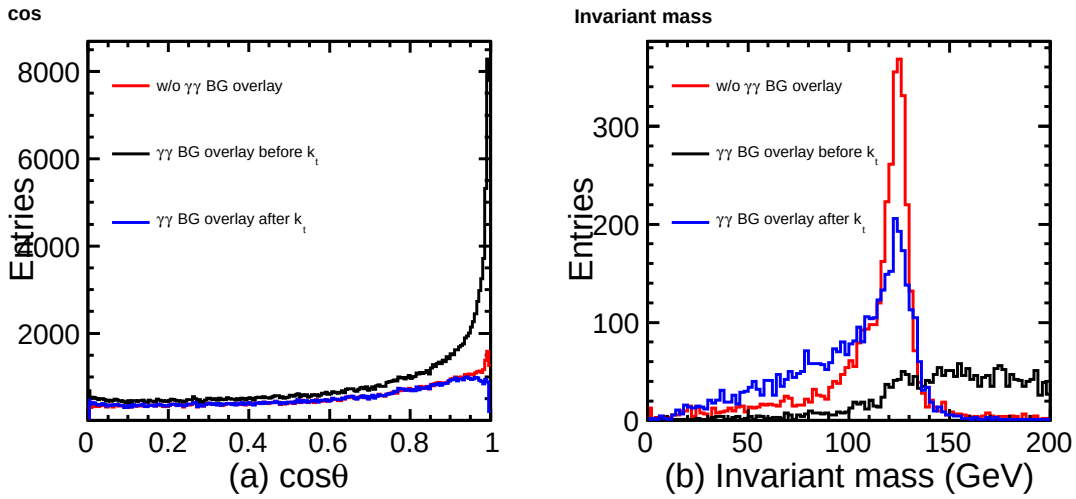

FIG. 4: $\gamma\gamma \to$ hadron background removal employing k_t jet algorithm on (a) $\cos\theta$ of PFOs and (b) invariant mass distribution in $\nu\bar{\nu}$h channel with or without background overlay.

distributed at the forward region are well subtracted as shown in Fig. 4 (a) and exceeded visible particles are suppressed shown in Fig 4 (b).

In k_t jet algorithm, following distance between particle i and j are calculated:

$$d_{ij} = \min(E_{ti}^2, E_{tj}^2) \cdot \frac{\Delta R_{ij}^2}{R^2} \tag{1}$$

where $\Delta R_{ij}^2 = (y_i - y_j)^2 + (\phi_i - \phi_j)^2$ and E_{ti}, y_{ij}, and ϕ_{ij} are a transverse momentum, rapidity, and azimuthal angle of $i-th$ particle and R is a jet-radius parameter. If d_{ij} is closed to the beam axis d_{ibeam}, these particles are merged as beam jet and these particles are treated as not related to any jets and removed. After removing $\gamma\gamma \to$ hadron backgrounds using k_t algorithm, flavor tagging

is performed for all the clustered particles employing `LCFIPlus` [12] implemented in `MarlinReco` package, which was coded in C++ and replaced from the previous `LCFIVertex` [13] implemented in FORTRAN. Neuralnet output for b and c quarks; Btag, Ctag, and their combination of BCtag (=Ctag/(Btag+Ctag)) from `LCFIPlus`, are used as input of flavor templates.

$$\mathrm{x-likeness} = \frac{\mathrm{x_1 x_2}}{\mathrm{x_1 x_2} + (1-\mathrm{x_1})(1-\mathrm{x_2})} \ (\mathrm{x = b,\ c,\ bc}), \tag{2}$$

where $\mathrm{x}_{1/2}$ is a neuralnet output of Btag, Ctag, and BCtag from LCFIPlus.

IV. $\mathrm{h} \to \mathrm{b\bar{b}},\ \mathrm{c\bar{c}},\ \mathrm{gg}$ CHANNEL ANALYSIS

A. Reconstruction and background reduction at $\sqrt{\mathrm{s}} = 1$ TeV

For the $\mathrm{h} \to \mathrm{b\bar{b}}$, $\mathrm{c\bar{c}}$, and gg channel analysis at the CM energy of 1 TeV, $\gamma\gamma \to$ hadrons background should be considered. At first forced two jet clustering is applied employing exclusive k_t algorithm selecting $R = 1.1$.

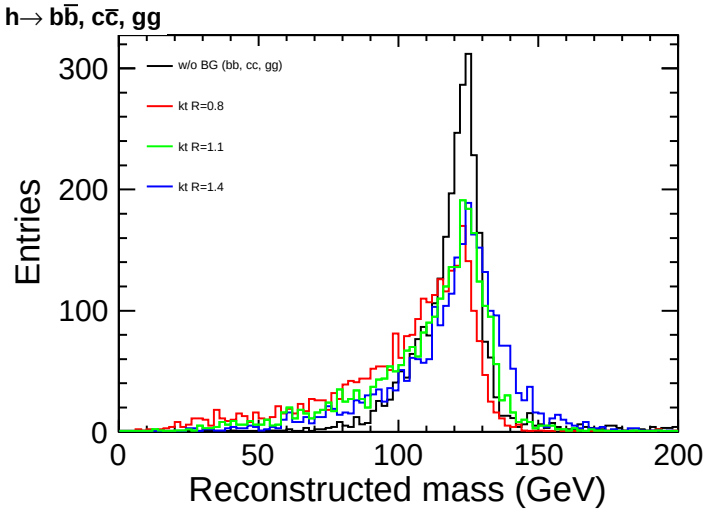

FIG. 5: Reconstructed Higgs mass distribution employing k_t jet clustering algorithm with different R parameters for $\mathrm{h} \to \mathrm{b\bar{b}},\ \mathrm{c\bar{c}},\ \mathrm{gg}$ selected by MC information.

After applying k_t jet clustering, `LCFIPlus` flavor tagging is applied for the particles clustered into jets and reclustered with jet clustering algorithm implemented in the `LCFIPlus` based on the Durham jet clustering algorithm [14]. After the reconstruction procedure, event selection and background reduction is performed for each cut condition, summarized on the Table III.

TABLE III: Cut flow summary of $h \to b\bar{b}$, $c\bar{c}$, gg channel analysis.

1. Visible energy on beam calorimeter	$E_{BCAL} < 50$ GeV
2. Thrust value	Thrust < 0.95
3. Visible energy	$100 < E_{vis} < 400$ GeV
4. Transverse visible momentum	$P_T > 50$ GeV
5. Number of charged particle flow object	$N_{ChdPFO} > 15$
6. Azimuthal angle of Higgs flight direction	$\lvert\cos\theta_h\rvert < 0.95$
7. Reconstructed dijet mass	$110 < M_{jj} < 150$ GeV

In order to identify the electrons or photons going into beam pipe direction from $e\gamma$ or $\gamma\gamma$ process, energy on the beam calorimeter (E_{BCAL}) is used to eliminate the two photon backgrounds event. Further reduction of huge $e\gamma$ processes is efficiently obtained by cut on the thrust variable defined as:

$$\text{Thrust } T = \max_{\vec{n}} \frac{\sum_i |\vec{p_i} \cdot \vec{n}|}{\sum_i |\vec{p_i}|},$$

where $\vec{p_i}$ is a momentum of i-th particle and $\vec{n}$ is an unit vector of the thrust axis which maximize the thrust value T.

Since $\nu\bar{\nu}$h final state has large missing energy and transverse momentum, cuts on the visible energy (E_{vis}) and visible transverse momentum (P_T) are applied to suppress fully hadronic decay and low P_T channels. Cuts on the number of charged particle flow objects (N_{ChdPFO}) and azimuthal angle of the flight direction of reconstructed Higgs ($\cos\theta_h$) are required to suppress the leptonic decay channels or particles going into forward region. Finally Higgs signals are selected with its mass range between 110 to 150 GeV. All the cut variables and cut conditions are shown in Fig. 6.

After passing all the selections, selection efficiencies are obtained as 35.0% ($h \to b\bar{b}$), 37.3% ($h \to c\bar{c}$), and 35.9% ($h \to gg$), respectively. An example of reconstructed Higgs mass distribution requiring additional b-likeness cut ($b-likeness > 0.6$) to select $h \to b\bar{b}$ is shown in Fig. 7. According to the Fig. 7, most of backgrounds are significantly eliminated by b-tagging.

In the DBD detector benchmarking study, both left- and right-handed $P(\mp 0.8, \pm 0.2)$ polarized beam runs are expected accumulating the integrated luminosity of same 500fb^{-1} with each polarization. From the Fig. 2 (b), even though main signal production process is significantly reduced, but WW-fusion production process is still achieved the largest cross section at 1 TeV with respect to the $P(+0.8, -0.2)$ beam polarization. Hence same cut conditions are adopted even for right-handed polarization to select WW-fusion production process. Background reduction on right-handed polarization are summarized in Table V.

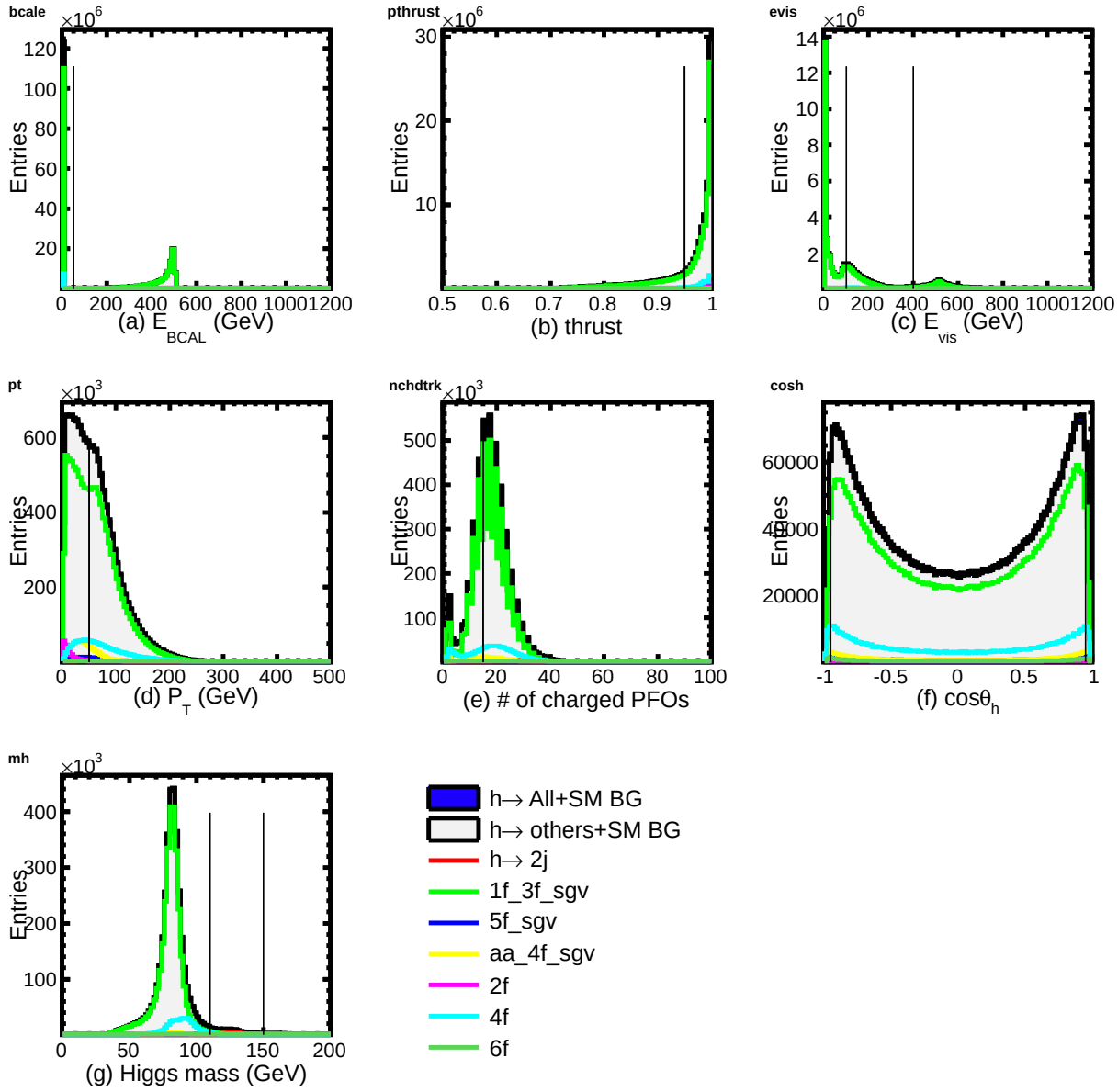

FIG. 6: Cut variables for h → 2j channel reconstruction with integrated luminosity of 500 fb^{-1} regarding P$(-0.8,\ +0.2)$ left-handed beam polarization.

B. Template fitting and accuracies of σBR

In order to evaluate the σBR with separating h → $b\bar{b}$, $c\bar{c}$, and gg, we apply the flavor template fitting to employ the flavor-likeness template calculated as Eq. 2.

After the all above selections, signal flavor templates of h → $b\bar{b}$, $c\bar{c}$, and gg and background template of the all other Higgs decay channels and SM background are prepared. In order to

TABLE IV: Summary table of cut flow for $h \to b\bar{b}$, $c\bar{c}$, and gg channel at $\sqrt{s} = 1$ TeV with $\mathcal{L} = 500$ fb^{-1} regarding $P(e^-,\ e^+) = P(-0.8,\ +0.2)$ polarization. Note that 3f, 5f, $\gamma\gamma \to 4f$ channels contributions were simulated and estimated using SGV fast simulation sample.

	Signals			Higgs other decays			
Cut flow	$h \to b\bar{b}$	$h \to c\bar{c}$	$h \to gg$	$h \to WW^*$	$h \to ZZ^*$	$h \to \tau\tau$	$h \to s\bar{s}$
No cut	128,700	6,058	19,045	48,320	5,979	14,291	90
1. E_{BCAL}	125,021	5,875	18,514	46,958	5,809	13,896	88
2. Thrust	104,305	4,910	15,506	35,780	4,569	10,248	80
3. E_{vis}	96,807	4,572	14,179	26,199	3,303	6,208	73
4. P_T	74,849	3,577	11,296	20,859	2,544	4,193	63
5. N_{ChdPFO}	70,005	3,152	11,133	16,402	2,074	113	50
6. $\lvert\cos\theta_h\rvert$	65,273	2,913	10,421	15,835	1,981	109	48
7. M_{jj}	44,988	2,258	6,845	4,419	685	32	41
Efficiency	35.0%	37.3%	35.9%	9.1%	11.5%	0.2%	45.7%

	SM backgrounds					
Cuts	3f	5f	$\gamma\gamma \to 4f$	2f	4f	6f
No cut	223,626,000	615,361	1,538,560	3,890,180	13,514,000	346,419
1. E_{BCAL}	110,066,000	498,059	1,374,030	3,354,840	8,473,960	318,340
2. Thrust	39,901,400	338,787	971,486	622,544	2,600,550	205,792
3. E_{vis}	10,449,800	203,570	662,748	208,035	1,233,480	64,422
4. P_T	5,595,070	102,081	225,666	13,986	782,962	48,951
5. N_{ChdPFO}	3,268,180	47,640	106,017	6,120	475,624	37,700
6. $\lvert\cos\theta_h\rvert$	3,175,530	38,739	94,914	4,076	441,836	33,997
7. M_{jj}	44,725	7,106	18,486	219	27,172	6,139
Efficiency	2.0×10^{-4}	1.2×10^{-2}	1.2×10^{-2}	5.6×10^{-5}	2.0×10^{-3}	1.8×10^{-2}

estimate the measurement accuracy of $\sigma BR(h \to s)$ ($s = b\bar{b},\ c\bar{c},\ gg$),

$$\sigma BR(s) = r_s \times \sigma BR^{SM}(s)\ (s = b\bar{b},\ c\bar{c},\ gg,\ bkg), \tag{3}$$

where $\sigma BR(s)$ and $\sigma BR^{SM}(s)$ are observed and expected products of cross section and branching ratio and r_s is a fluctuation from the SM prediction. From the Eq. 3, the measurement accuracy of $\sigma BR(s)$ is estimated as

$$\frac{\Delta\sigma BR(h \to s)}{\sigma BR} = \frac{\Delta r_s}{r_s}. \tag{4}$$

Relative uncertainties of the r_s are estimated with the binned log-likelihood fitting for flavor

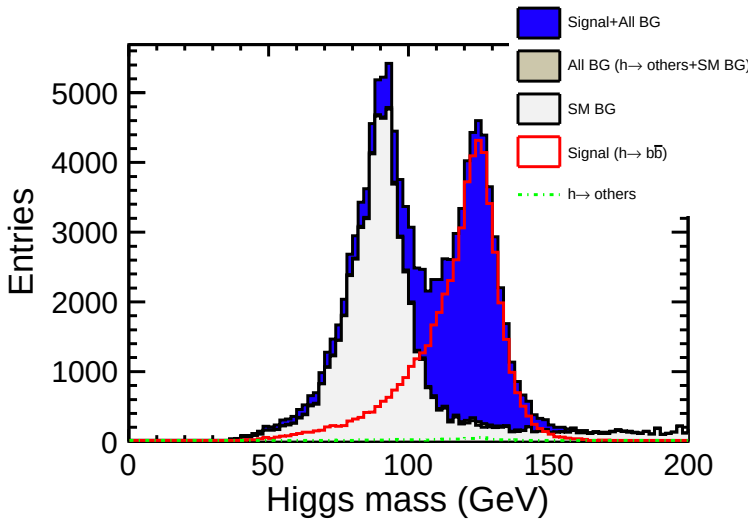

FIG. 7: Example of the reconstructed Higgs mass distribution at $\sqrt{s} = 1$ TeV in $h \to b\bar{b}$ channel assuming the b-likeness cuts ($b-likeness > 0.6$).

templates. Assuming the Poisson statistics, probability of entry in each bin is determined as;

$$P_{ijk} = \frac{\mu^n e^{-\mu}}{n!}, \tag{5}$$

where $n \equiv N_{ijk}^{data}$ is a expected number of data entries in (i, j, k) bin, and μ represents the sum of each template sample entries at (i, j, k) bin, which is defined as $N_{ijk}^{template}$:

$$N_{ijk}^{template} = \sum_{s=bb,\ cc,\ gg} r_s \cdot N_{ijk}^{s} + N_{ijk}^{bkg}, \tag{6}$$

where N_{ijk}^{s} is a number of entries in each template bin predicted in SM and N_{ijk}^{bkg} is a sum of entries from $h \to$ others and SM backgrounds in (i, j, k) bin. Two dimensional images of the three dimensional $b-$, $c-$, and $bc-$ flavor-likeness template samples for $h \to b\bar{b}$, $c\bar{c}$, gg, others, and SM backgrounds are shown in Fig. 8.

The uncertainty of the r_s is evaluated by the 5,000 times of Toy-MC with log-likelihood fitting by fluctuating the Data samples assuming the Poisson statistics in each bin. After applying template fitting, accuracies of σBR are extracted from the Gaussian fitting for parameter r_s.

Fitted results and extracted accuracies of σBRs assuming the integrated luminosity of $\mathcal{L} = 500\ fb^{-1}$ with both beam polarization $P(e^-,\ e^+) = P(\mp 0.8,\ \pm 0.2)$ are summarized on the Table VI.

Concerning the precision measurement of the Higgs boson σBRs, left-handed beam polarization $P(-0.8,\ +0.2)$ with accumulating the integrated luminosity of $\mathcal{L} = 1\ ab^{-1}$ is also evaluated on the same table. Note that these results are only considered the statistical uncertainty of σBR.

TABLE V: Summary table of background reduction for $h \to b\bar{b}$, $c\bar{c}$, and gg at $\sqrt{s} = 1$ TeV with $\mathcal{L} = 500$ fb^{-1} and $P(e^-,\ e^+) = P(+0.8,\ -0.2)$ right-handed beam polarization. Note that 3f, 5f, $\gamma\gamma \to$ 4f channels contributions were simulated and estimated using SGV fast simulation sample.

	Signal			Other Higgs decays			
Cut flow	$h \to b\bar{b}$	$h \to c\bar{c}$	$h \to gg$	$h \to WW^*$	$h \to ZZ^*$	$h \to \tau\tau$	$h \to s\bar{s}$
No cut	17,768	812	2,566	6,592	830	1,992	10
1. E_{BCAL}	17,054	783	2,463	6,331	794	1,917	9
2. Thrust	10,999	512	1,628	3,743	457	1,068	7
3. E_{vis}	8,049	366	1,152	2,230	282	567	6
4. P_T	6,045	284	898	1,722	211	377	5
5. N_{ChdPFO}	5,608	248	882	1,328	171	24	4
6. $\lvert\cos\theta_h\rvert$	5,171	224	815	1,262	157	21	4
7. M_{jj}	3,542	172	537	354	56	4	3
Efficiency	19.9%	21.2%	20.9%	5.4%	6.7%	0.2%	29.5%

	SM backgrounds					
Cut flow	3f	5f	$\gamma\gamma \to$ 4f	2f	4f	6f
No cut	205,529,000	415,380	1,538,560	2,699,560	6,530,160	119,252
1. E_{BCAL}	92,815,300	310,618	1,374,030	2,288,410	2,174,560	103,473
2. Thrust	28,610,000	206,465	971,486	401,722	606,529	67,684
3. E_{vis}	4,870,840	131,761	662,748	135,701	252,878	17,727
4. P_T	1,947,590	60,325	225,666	8,963	130,966	12,774
5. N_{ChdPFO}	1,095,980	28,418	106,017	2,634	74,999	10,265
6. $\lvert\cos\theta_h\rvert$	1,060,520	23,195	94,914	1,497	69,081	9,228
7. M_{jj}	15,749	4,417	18,486	144	3,493	1,575
Efficiency	7.7×10^{-5}	1.1×10^{-2}	1.2×10^{-2}	5.3×10^{-5}	5.3×10^{-4}	1.3×10^{-2}

V. $h \to WW^*$ CHANNEL ANALYSIS

In the $h \to WW^*$ analysis, high energetic neutrinos are generated via the production process of $\nu\bar{\nu}h$, therefore $h \to WW^*$ fully hadronic decay channel ($h \to WW^* \to q\bar{q}q\bar{q}$) is analyzed with reconstructing four jet final state.

In order to suppress the $\gamma\gamma \to$ hadron backgrounds, exclusive four jet clustering with k_t algorithm is applied for selecting $R = 0.9$. Owing to this algorithm, beam related backgrounds are well removed, then LCFIPlus flavor tagging is applied for all the reconstructed particles and re-clustered as four jets forcibly by Durham [14] base jet clustering in the LCFIPlus package.

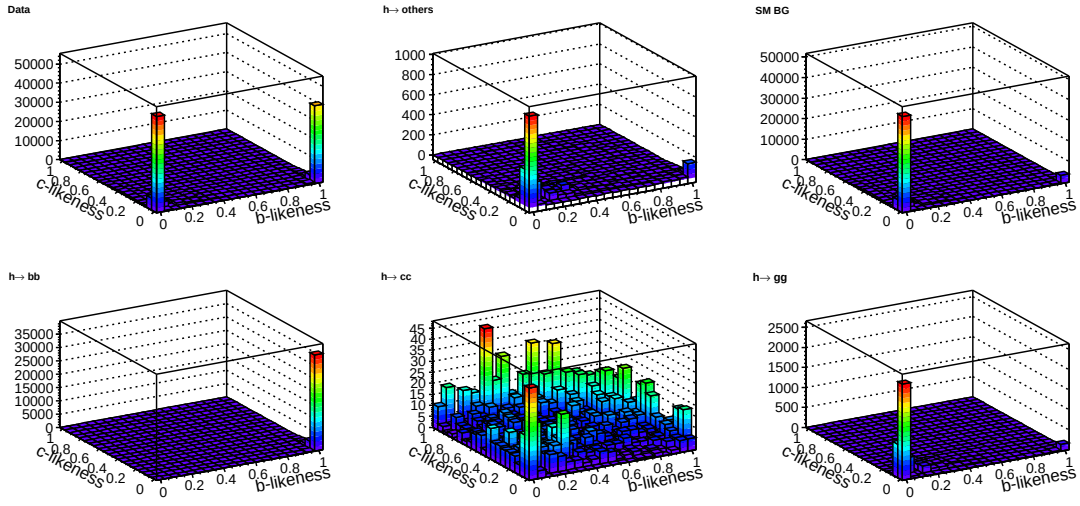

FIG. 8: 2D image of the 3D flavor template samples for Data, $h \to b\bar{b}$, $c\bar{c}$, gg, others, and SM BGs.

TABLE VI: Estimated measurement accuracies of σBR for $h \to b\bar{b}$, $c\bar{c}$, and gg channels at $\sqrt{s} = 1$ TeV with respect to the $\mathcal{L} = 500$ fb^{-1} for both P(e^-, e^+) = (∓ 0.8, ± 0.2) beam polarizations or accumulating $\mathcal{L} = 1$ ab^{-1} regarding P(-0.8, $+0.2$) left-handed polarization. Here these results are taken only statistical uncertainties into account.

Integrated luminosity	500 fb^{-1}	500 fb^{-1}	1 ab^{-1}
Beam polarization P(e^-, e^+)	P(-0.8, $+0.2$)	P($+0.8$, -0.2)	P(-0.8, $+0.2$)
r_{bb}	1.000±0.005	0.999±0.021	1.000±0.004
r_{cc}	1.002±0.057	1.034±0.380	1.001±0.039
r_{gg}	0.998±0.039	1.025±0.263	0.998±0.028
$\Delta\sigma$BR/σBR($h \to b\bar{b}$)	0.54%	2.1%	0.39%
$\Delta\sigma$BR/σBR($h \to c\bar{c}$)	5.7%	36.8%	3.9%
$\Delta\sigma$BR/σBR($h \to gg$)	3.9%	25.7%	2.8%

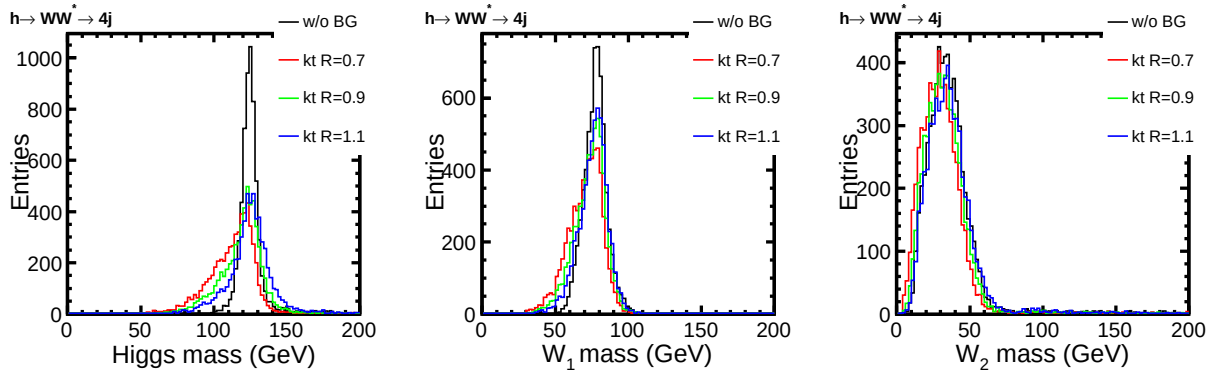

FIG. 9: Four jet reconstruction employing k_t algorithm with different R parameters.

At the Higgs mass of 125 GeV, one W should be off-shell and only one W has mass close to the W mass (M_W). The best jet pair combination is selected as closest dijet mass as M_W, which has minimum mass difference of $|M_{jj} - M_W|$. Selected W candidate is defined as W_1 and remaining dijet is described as W_2, where they are mostly contributed from on-shell and off-shell W, respectively. After the jet clustering and pairing, following cuts are applied to suppress SM backgrounds and other Higgs decay channel contributions.

TABLE VII: Cut flow summary of $h \to WW^*$ channel analysis.

1.	Visible energy on beam calorimeter	$E_{BCAL} < 50$ GeV
2.	Thrust	Thrust < 0.95
3.	Visible energy	$100 < E_{vis} < 400$ GeV
4.	Visible transverse momentum	$P_T > 50$ GeV
5.	Total number of charged particle flow object	$N_{ChargedPFO} > 25$
6.	Azimuthal angle of each jet	$\lvert\cos\theta_j\rvert < 0.90$
7.	Y_{34} value	$-\log_{10}(Y_{34}) < 3.0$
8.	Y_{23} value	$-\log_{10}(Y_{23}) < 2.2$
9.	Sum of B-tagging output for four jets	$Btag_{4j} < 0.8$
10.	W_1 mass (Closest to M_W)	$60 < M_{W_1} < 95$ GeV
11.	W_2 mass (Remaining dijet mass)	$15 < M_{W_2} < 60$ GeV
12.	Higgs mass	$110 < M_h < 140$ GeV

First requiring energetic jets final state to suppress semi-leptonic decay channels in 2f and 4f (WW, ZZ) requiring large visible energy and transverse momentum. In addition, cut on N_{PFO} and N_j are required to suppress the leptonic and semileptonic decay channel from $WW \to \ell\nu qq$. Cuts on the threshold value of jet clustering y value used in the Durham jet algorithm from i to j=i+1 jets ($-\log_{10}(Y_{ij})$) are applied to reduce non-four jets like events. In order to suppress the other Higgs decay channels contribution, mostly comes from the $h \to b\bar{b}$ by largest fraction of the Higgs decay; sum of Btag output for four jets is required ($Btag_{4j} < 0.8$). After applying b-tagging cut, remaining contribution from other Higgs decay channel is mainly coming from $h \to gg$.

Reconstructed Higgs mass distribution regarding $h \to WW^*$ hadronic decay channel is shown in Fig. 11. P(+0.8, − 0.2) right-handed beam polarization running with the same integrated luminosity of 500 fb^{-1} is also estimated. According to the right-handed electron beam polarization, production process via $WW-$fusion contributed by the t-channel diagram is suppressed, hence both main signal production channel $\nu_e\bar{\nu}_e h$ and WW background productions are reduced.

Therefore, same cut flow is applied as left-handed polarization case which optimized for WW-

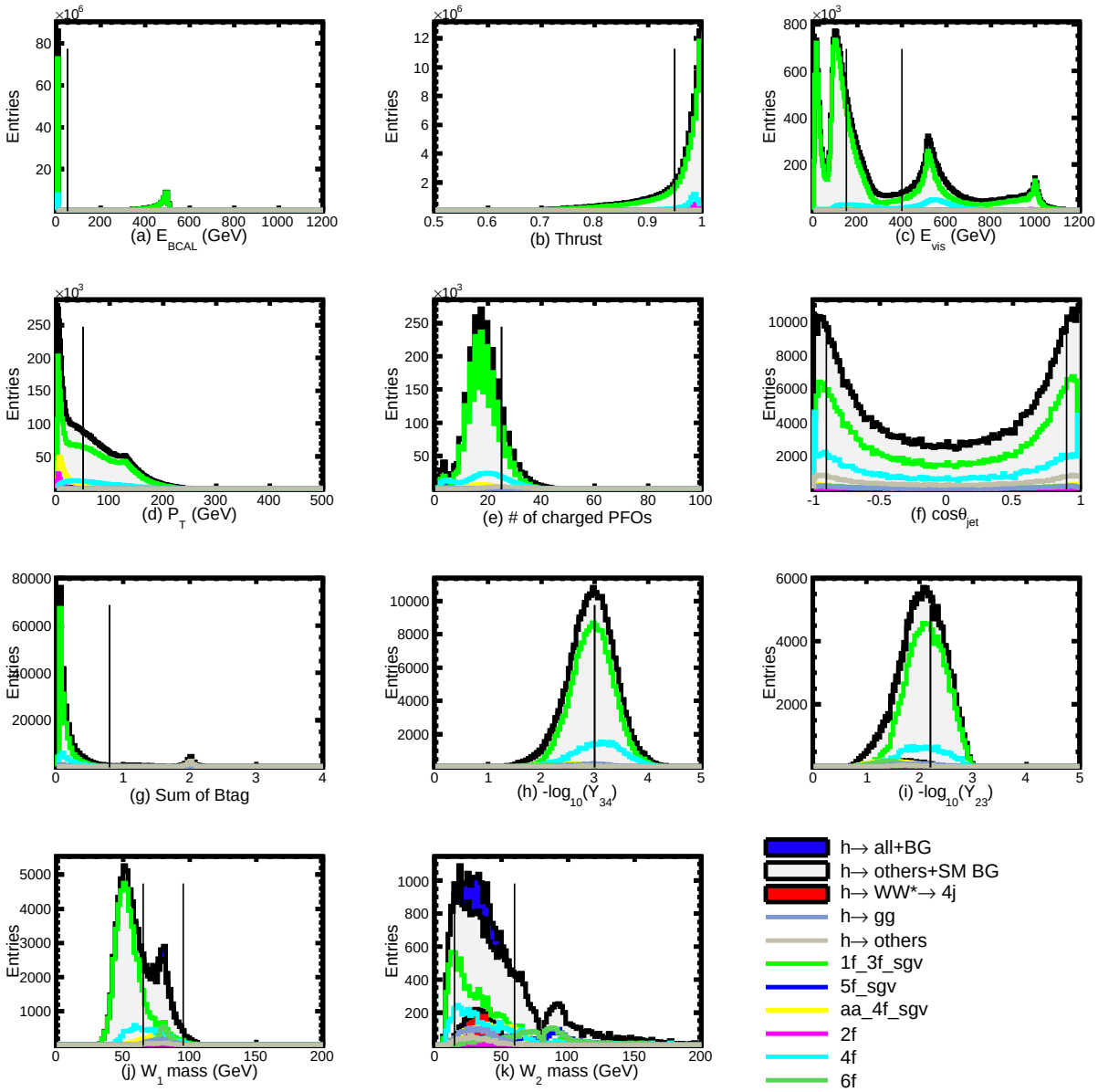

FIG. 10: Cut variables of h → WW* analysis.

fusion process. Backgrounds reductions are summarized on the Table VIII and IX.

After passing all the selections, signal significance $S/\sqrt{(S+B)}$, where S is a number of selected signal samples and B is a total number of background samples; is obtained from the final selected samples as 27.9 with P$(-0.8,\ 0.2)$ left-handed and 4.2 with P$(+0.8,\ -0.2)$ right-handed beam polarizations assuming the same integrated luminosity of $\mathcal{L} = 500$ fb^{-1}.

As a result, $\Delta\sigma$BR$/\sigma$BR(h → WW*) is estimated as 3.6% with P$(-0.8,\ +0.2)$ and 23.7% with P$(+0.8,\ -0.2)$ polarizations. Assuming further statistics of 1 ab^{-1} only running with P$(-0.8,\ +0.2)$ left-handed polarization, measurement accuracy is expected to be improved as 2.5%. Note that

TABLE VIII: Summary table of background reduction on $h \to WW^* \to 4j$ channel assuming $\mathcal{L} = 500$ fb^{-1} with respect to the P(-0.8, $+0.2$) left-handed beam polarization at $\sqrt{s} = 1$ TeV. Note that 3f, 5f, $\gamma\gamma \to$ 4f channels contributions were simulated and estimated using SGV fast simulation sample.

	Signal	Other Higgs decays					
Cut flow	$h \to WW^* \to 4j$	$h \to b\bar{b}$	$h \to c\bar{c}$	$h \to gg$	$h \to ZZ^*$	$h \to \tau\tau$	$h \to s\bar{s}$
No cut	21,976	128,700	6,058	19,045	5,979	14,291	90
1. E_{BCAL}	21,348	124,986	5,873	18,514	5,797	13,747	88
2. Thrust	19,256	109,860	5,188	16,530	5,006	11,601	84
3. E_{vis}	14,534	82,950	4,108	12,709	2,924	4,828	66
4. P_T	12,185	67,792	3,375	10,607	2,341	3,388	61
5. N_{ChdPFO}	8,992	38,071	1,534	9,115	1,350	32	24
6. $\lvert\cos\theta_j\rvert$	5,330	20,555	868	5,325	782	10	15
7. $Btag_{4j}$	5,027	651	769	4,958	501	6	15
8. $-\log Y_{34}$	4,363	304	289	2,916	420	5	6
9. $-\log Y_{23}$	3,792	215	203	2,034	348	3	4
10. M_{W1}	3,177	162	167	1,684	280	2	3
11. M_{W2}	3,025	140	145	1,539	257	2	3
12. M_h	2,732	118	124	1,366	231	1	3
Efficiency	12.4%	0.1%	2.0%	7.2%	3.9%	0.0%	3.1%

	SM backgrounds					
Cut flow	3f	5f	$\gamma\gamma \to 4f$	2f	4f	6f
No cut	223,628,000	615,361	1,538,560	3,890,180	13,514,000	346,419
1. E_{BCAL}	72,750,600	483,560	1,284,930	3,347,830	8,442,530	317,394
2. Thrust	23,633,100	408,482	1,102,330	771,237	2,929,920	260,408
3. E_{vis}	4,967,370	105,205	606,486	133,143	803,488	30,640
4. P_T	2,750,240	38,794	95,691	6,925	524,360	22,308
5. N_{ChdPFO}	289,052	7,034	11,092	171	112,904	12,726
6. $\lvert\cos\theta_j\rvert$	170,938	3,393	5,782	60	48,634	7,736
7. $Btag_{4j}$	168,176	3,227	5,641	25	35,396	3,946
8. $-\log Y_{34}$	89,374	2,882	4,746	13	15,194	3,395
9. $-\log Y_{23}$	51,723	2,716	4,395	13	9,464	3,249
10. M_{W1}	8,879	2,397	3,400	13	4,889	3,005
11. M_{W2}	6,064	792	2,369	0	3,350	783
12. M_h	2,568	164	850	0	1,206	113
Efficiency	1.1×10^{-5}	2.7×10^{-4}	5.5×10^{-4}	0.0	8.9×10^{-5}	3.2×10^{-4}

TABLE IX: Summary table of background reduction in $h \to WW^* \to 4j$ channel assuming $\mathcal{L} = 500$ fb^{-1} with respect to the P(+0.8, −0.2) right-handed beam polarization at $\sqrt{s} = 1$ TeV. Note that 3f, 5f, $\gamma\gamma \to 4f$ channels contributions were simulated and estimated using SGV fast simulation sample.

	Signal	Other Higgs decays					
Cut values	$h \to WW^* \to 4j$	$h \to b\bar{b}$	$h \to c\bar{c}$	$h \to gg$	$h \to ZZ^*$	$h \to \tau\tau$	$h \to ss$
No cut	2,972	17,768	812	2,566	830	1,992	10
1. E_{BCAL}	2,870	17,048	782	2,463	794	1,906	9
2. Thrust	2,055	12,071	559	1,824	527	1,259	7
3. E_{vis}	1,126	6,456	315	981	242	430	5
4. P_T	928	5,218	255	811	191	302	5
5. N_{ChdPFO}	683	2,921	116	698	109	7	2
6. $\lvert\cos\theta_j\rvert$	405	1,589	67	411	64	3	1
7. $Btag_{4j}$	381	48	58	382	39	3	1
8. $-\log Y_{34}$	327	22	21	221	32	2	0
9. $-\log Y_{23}$	284	16	15	155	27	1	0
10. M_{W_1}	237	12	12	128	22	1	0
11. M_{W_2}	212	10	10	107	19	1	0
12. M_h	193	8	9	95	17	0	0
Efficiency	6.5%	0.0%	1.1%	3.7%	2.1%	0.0%	0.0%

	SM backgrounds					
Cut values	3f	5f	$\gamma\gamma \to 4f$	2f	4f	6f
No cut	205,530,000	415,380	1,538,560	2,699,560	6,530,160	119,252
1. E_{BCAL}	60,587,000	301,833	1,284,930	2,282,960	2,155,180	103,093
2. Thrust	15,111,000	249,963	1,102,330	486,424	626,178	82,263
3. E_{vis}	2,317,670	69,903	606,486	87,755	143,697	6,761
4. P_T	935,773	21,219	95,691	5,672	74,944	4,289
5. N_{ChdPFO}	96,284	3,251	11,092	117	13,979	2,712
6. $\lvert\cos\theta_j\rvert$	56,987	1,454	5,782	28	4,744	1,691
7. $Btag_{4j}$	56,091	1,387	5,641	25	3,606	491
8. $-\log Y_{34}$	29,965	1,245	4,746	13	1,641	440
9. $-\log Y_{23}$	17,261	1,171	4,395	13	1,033	421
10. M_{W_1}	3,057	1,006	3,400	13	531	390
11. M_{W_2}	1,801	269	1,796	0	320	62
12. M_h	766	79	769	0	143	12
Efficiency	3.7×10^{-6}	1.9×10^{-4}	5.0×10^{-4}	0.0	2.2×10^{-5}	1.0×10^{-4}

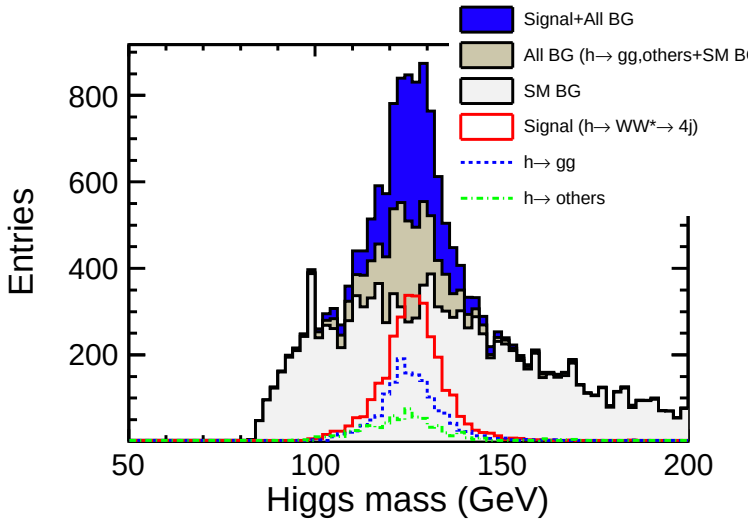

FIG. 11: Reconstructed Higgs mass distribution for h → WW* hadronic decay channel at $\sqrt{s} = 1$ TeV with respect to the $\mathcal{L} = 500$ fb^{-1} with P$(-0.8, +0.2)$ beam polarization.

TABLE X: Measurement accuracies of σBR in h → WW* → 4j channel with respect to the $\mathcal{L} = 500$ fb^{-1} for both P$(\mp 0.8, \ \pm 0.2)$ beam polarizations or accumulating $\mathcal{L} = 1$ ab^{-1} regarding P$(-0.8, \ +0.2)$ left-handed polarization.

Integrated luminosity	500 fb^{-1}	500 fb^{-1}	1 ab^{-1}
Beam polarization P(e$^-$, e$^+$)	P$(-0.8, \ +0.2)$	P$(+0.8, \ -0.2)$	P$(-0.8, \ +0.2)$
Signal significance $(S/\sqrt{S+B})$	27.9	4.2	39.7
$\Delta\sigma$BR/σBR(h → WW* → 4j)	3.6%	23.7%	2.5%

current cut based analysis still remains h → gg and ZZ contribution after the all cuts but not taken into account for the systematic uncertainty of σBR(h → WW*). Further improvement is needed to reduce the uncertainty from other Higgs decay channels.

VI. CONCLUSION

Measurement accuracies of the σBR for the Higgs decay channels of h → b$\bar{\text{b}}$, c$\bar{\text{c}}$, gg, and WW* → 4j are analyzed at the CM energy of 1 TeV. All results are summarized on Table XI assuming the $\mathcal{L} = 500$ fb^{-1} and 1 ab^{-1} regarding both P$(\mp 0.8, \pm 0.2)$ beam polarizations. Owing to the good background separation by B-tagging, h → b$\bar{\text{b}}$ channel can also achieve good situation even with right-handed polarization, but that is degraded for other channel case significantly, which is mainly caused by $e\gamma \to \nu qq$ or $\gamma\gamma \to qqqq$. h → cc, gg, WW* are affected by this background except for the h → bb. $\gamma\gamma \to qqqq$ contribution is relatively increased with the right-handed beam

polarization case. Note that all the results are only considered statistical uncertainty of σBR and systematic uncertainty from other decays and backgrounds should be also taken into account in further study.

TABLE XI: Summary table of the measurement accuracies of σBR at $\sqrt{s} = 1$ TeV assuming $\mathcal{L} = 500$ fb^{-1} with $P(\mp 0.8, \ \pm 0.2)$ both polarizations or 1 ab^{-1} only accumulating P$(-0.8, \ +0.2)$ left-handed beam polarization. Results are only considered statistical uncertainty.

Integrated luminosity	500 fb^{-1}		1 ab^{-1}
Beam polarization P(e^-, e^+)	P$(-0.8, \ +0.2)$	P$(+0.8, -0.2)$	P$(-0.8, \ +0.2)$
$\Delta\sigma$BR/σBR($h \to b\bar{b}$)	0.54%	2.1%	0.39%
$\Delta\sigma$BR/σBR($h \to c\bar{c}$)	5.7%	36.8%	3.9%
$\Delta\sigma$BR/σBR($h \to gg$)	3.9%	25.7%	2.8%
$\Delta\sigma$BR/σBR($h \to WW^* \to 4j$)	3.6%	23.7%	2.5%

Acknowledgments

We would like to acknowledge the members who join the ILD Analysis and Software meeting [16] for useful discussion of this work and to ILD software task group members who maintain the analysis tools and MC samples for DBD detector benchmarking study. Especially, Mikael Berggren, Jenny List, and Akiya Miyamoto for useful discussion and suggestion for this analysis, Frank Gaede and Jan Engels for production and manage large amount of simulation/reconstruction samples.

VII. BIBLIOGRAPHY

[1] The ATLAS Collaboration, Phys. Lett. B 710, 49 (2012).

[2] The CMS Collaboration, Phys. Lett. B 710, 26 (2012).

[3] T. Abe et al. [ILD Concept Group - Linear Collider Collaboration], "The International Large Detector: Letter of Intent", KEK Report 2009-6.

[4] LHC Higgs Cross Section Working Group, arXiv:1101.0593v3 [hep-ph] (2011).

[5] W. Kilian *et al.*, arXiv:0708.4233 [hep-ph]
M. Moretti *et al.*, arXiv: 0102.195-rev [hep-ph].

[6] http://ilcsoft.desy.de/portal/.

[7] P. Mora de Freitas and H. Videau, LC-TOOL-2003-010, Prepared for LCWS 2002,. Jeju Island, Korea, 26-30 Aug 2002.

[8] O. Wendt and F. Gaede and T. Krämer, arXiv:physics/0702171v1 [physics.ins-det].

[9] M. Berggren, arXiv:1203.0217v1 [physics.ins-det] (2012).

[10] Matteo Cacciari, Gavin P. Salam, Gregory Soyez, arXiv:1111.6097v1 [hep-ph] (2011).

[11] Detailed Baseline Design document ILD section, http://ific.uv.es/ fuster/DBD-Chapters/Chapter4 ILD.pdf

[12] https://confluence.slac.stanford.edu/display/ilc/LCFIPlus.

[13] Nuclear Instruments and Methods in Physics Research Section A, Volume 610, Issue 2, p. 573-589.

[14] S. Catani *et al.*, Phys. Lett. B 269, 432-438 (1991)

[15] http://www-jlc.kek.jp/subg/physics/ilcphys/

[16] http://ilcagenda-beta.linearcollider.org/categoryDisplay.py?categId=131

[17] T. Sjöstrand, S. Mrenna and P. Skands, JHEyP05 (2006) 026.

Appendix

Appendix A: Higgs BR study at 500 GeV

1. Reconstruction and background reduction at 500 GeV

At the CM energy of 500 GeV, large amount of reconstructed signal and SM background samples are available for which were produced the study of ILD Letter of Intent (LOI), even though these samples were generated employing the Higgs mass of 120 GeV in `whizard-1.40`. Higgs BRs are calculated by `Pythia` [17] instead of used in DBD analysis, where the BRs for $h \to b\bar{b}$, $c\bar{c}$, and gg are $BR(h \to b\bar{b}) = 65.7\%$, $BR(h \to c\bar{c}) = 3.6\%$, and $BR(h \to gg) = 5.5\%$, respectively. These generated samples are also simulated with previous `ILD_00` detector model in Mokka. For the flavor tagging, `LCFIVertex` package [13] was used. In the $h \to b\bar{b}$, $c\bar{c}$, and gg reconstruction, `Durham` jet clustering [14] was applied and forcibly clustered as two jet. Note that at the $\sqrt{s} = 500$ GeV, $\gamma\gamma$ beam induced background contribution is relatively smaller than 1 TeV, thus $\gamma\gamma \to$ hadron backgrounds were not overlaid to the samples.

In order to select the $\nu_e\bar{\nu}_e h$ WW-fusion process, at first cut on missing mass is applied to suppress Zh process. Cuts on P_T, P_Z, P_{max}, and N_{chd} are required to suppress semi-leptonic decay channels. Finally Higgs signal is selected with the cut on reconstructed Higgs mass region.

TABLE XII: Cut flow for $\sqrt{s} = 500$ GeV analysis

1. Missing mass	$M_{miss} > 220$ GeV
2. Transverse visible momentum	$P_T > 20$ GeV
3. Longitudinal visible momentum	$\|P_Z\| < 150$ GeV
4. Maximum momentum PFO	$P_{max} < 50$ GeV
5. Number of charged tracks	$N_{chd} > 10$
6. Reconstructed Higgs mass	$100 < M_h < 130$ GeV

TABLE XIII: Background reduction summary at $\sqrt{s} = 500$ GeV with $\mathcal{L} = 500$ fb^{-1} regarding P$(-0.8,\ +0.3)$ beam polarization. $\nu\nu\ell\ell$ and $\ell\ell\ell\ell$ processes are completely suppressed.

Cuts	$h \to bb$	$h \to c\bar{c}$	$h \to gg$	$h \to$ all	$\nu\bar{\nu}q\bar{q}$	$\nu\ell q\bar{q}$	$\ell\ell qq$	qqqq	ZWW	ZZZ
Gen	59,921	3,336	5,053	90,029	367,779	5,042,400	682,517	4,288,940	513,824	2,681
1	51,619	2,811	4,185	78,712	239,835	192,350	3,739	114,929	28,140	1,068
2	47,889	2,629	4,017	72,087	213,867	155,999	1,230	43,028	26,009	927
3	46,431	2,552	3,895	69,132	197,487	134,599	1,136	42,930	25,679	910
4	43,604	2,308	3,711	61,308	175,734	58,380	613	15,006	16,581	777
5	43,307	2,280	3,711	57,126	166,037	56,281	610	14,976	15,894	699
6	35,054	2,040	3,711	45,473	15,405	16,657	90	663	4,372	226
Efficiency	55.6%	46.0%	64.5%	41.2%	1.7×10^{-2}	2.2×10^{-3}	1.5×10^{-4}	1.7×10^{-4}	7.1×10^{-3}	7.4×10^{-2}

2. Measurement accuracies of σBR at the $\sqrt{s} = 500$ GeV

After applying all above cuts, flavor templates on $h \to b\bar{b}$, $c\bar{c}$, and gg are prepared using the Neuralnet-output for b, c, bc flavor from `LCFIVertex`. 5,000 times of Toy-MC is applied and extracted the accuracies of σBR. Fitted results by template fitting Toy-MC are shown in Fig. 12 and summarized on the Table XIV.

FIG. 12: Fitted r_s distribution for $h \to b\bar{b}$, $c\bar{c}$, and gg at $\sqrt{s} = 500$ GeV with assuming the $\mathcal{L} = 500$ fb^{-1} and P$(-0.8,\ +0.3)$ left-handed beam polarization.

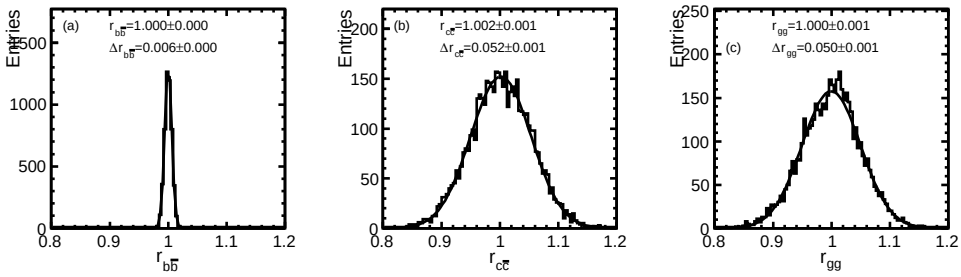

TABLE XIV: Reduction summary for $h \to b\bar{b}$, $c\bar{c}$, gg channels at $\sqrt{s} = 500$ GeV assuming $\mathcal{L} = 500$ fb^{-1} and P$(-0.8,\ +0.3)$ beam polarization at the Higgs mass of 120 GeV.

Integrated luminosity	500 fb^{-1}
Beam polarization P$(e^-,\ e^+)$	P$(-0.8,\ +0.3)$
r_{bb}	1.000 ± 0.006
r_{cc}	1.002 ± 0.052
r_{gg}	1.000 ± 0.050
$\Delta\sigma BR/\sigma BR(h \to b\bar{b})$	0.6%
$\Delta\sigma BR/\sigma BR(h \to c\bar{c})$	5.2%
$\Delta\sigma BR/\sigma BR(h \to gg)$	5.0%